**VTT Technical Research Centre of Finland**

# ERO modelling of net and gross erosion of marker samples exposed to L-mode plasmas on ASDEX Upgrade

Hakola, Antti; Keitaanranta, A.; Kumpulainen, Heikki; Lahtinen, Aapeli; Likonen, Jari; Balden, M.; Cavedon, M.; Krieger, K.; Airila, Markus; Groth, M.; ASDEX Upgrade Team; EUROfusion MST1 Team

*Published in:*
Nuclear Materials and Energy

*DOI:*
10.1016/j.nme.2020.100863

Published: 01/12/2020

*Document Version*
Publisher's final version

Nuclear Materials and Energy 25 (2020) 100863

Contents lists available at ScienceDirect

Nuclear Materials and Energy

journal homepage: www.elsevier.com/locate/nme

# ERO modelling of net and gross erosion of marker samples exposed to L-mode plasmas on ASDEX Upgrade

A. Hakola [a,*], A. Keitaanranta [b], H. Kumpulainen [b], A. Lahtinen [c], J. Likonen [a], M. Balden [d], M. Cavedon [d], K. Krieger [d], M. Airila [a], M. Groth [b], ASDEX Upgrade Team[e], EUROfusion MST1 Team[e]

[a] VTT, P. O. Box 1000, 02044 VTT, Finland
[b] Aalto University, P. O. Box 11000, 00076 AALTO, Finland
[c] University of Helsinki, Department of Physics, P.O. Box 43, 00014 University of Helsinki, Finland
[d] Max-Planck-Institut für Plasmaphysik, 85748 Garching, Germany
[e] See author list of H. Meyer et al. 2019 Nucl. Fusion 59 112014
[f] See author list of B. Labit et al. 2019 Nucl. Fusion 59 086020

ARTICLE INFO

*Keywords:*
Erosion
Material migration
ASDEX Upgrade
L-mode
Marker samples

ABSTRACT

In this paper, we report experimental and numerical investigations of gross and net erosion of gold (Au) and molybdenum (Mo), proxies for the common plasma-facing material tungsten (W), during L-mode plasma discharges in deuterium (D) in the outer strike-point region of the ASDEX Upgrade tokamak. To this end, erosion profiles of different marker spots (for Au, dimensions 1 × 1 and 5 × 5 mm$^2$) and marker coatings (for Mo) have been determined and modelled using the ERO code. The smaller marker spots were designed to quantify the gross-erosion rate while on the bigger markers local prompt re-deposition of Au allowed obtaining data on net erosion.

The experimental results indicate relatively uniform erosion profiles across the marker spots or coatings, very little re-deposition elsewhere, and the largest erosion taking place close to the strike point. Compared to W, the markers show up to 15 times higher net erosion but no major differences in the poloidal migration lengths of Au and W can be seen. Gold thus appears to be a proper choice for studying migration of W in the divertor region.

The ERO simulations with different background plasmas are able to reproduce the main features of the experimental net erosion profile of Au. Of the studied parameters, electron temperature has the strongest impact on erosion: doubling the temperature enhances erosion by a factor of 2.5–3. In contrast, for Mo, the simulated net erosion is ~ 3 times smaller than what experimental data indicate. The discrepancies can be attributed to the deviations of the background plasma profiles from the measured ones as well as to the applied models or approximations for the ion temperature, plasma potential, and sheath characteristics in ERO. In addition, the surrounding areas of the marker samples being covered with impurities and W from previous experiments may have considerably reduced the actual re-deposition of Mo.

All the simulations predict a toroidal tail of re-deposited particles, downstream of the markers, but the particle density seems to be below the experimental detection threshold. The comparison between the 1 × 1 mm$^2$ and 5 × 5 mm$^2$ marker spots further reveal that re-deposition drops from >50% to <40% when decreasing the marker size. This indicates that small enough marker samples can be used for accurately determining gross erosion in ASDEX Upgrade.

## 1. Introduction

Understanding erosion of tungsten (W) plasma-facing components (PFCs) is crucial for successful operation of future fusion reactors. The smaller the erosion during normal plasma operation and off-normal events is, the larger will be the lifetime of the PFCs, the fewer will be the number of heavy impurities accumulating in the plasma core, and the better can the formation of tritium-rich co-deposited layers be

* Corresponding author.
*E-mail address:* antti.hakola@vtt.fi (A. Hakola).

https://doi.org/10.1016/j.nme.2020.100863
Received 31 July 2020; Received in revised form 25 November 2020; Accepted 27 November 2020
Available online 1 December 2020

controlled [1,2]. For the latter two goals, it is also important is to identify key material migration processes in the edge and scrape-off layer (SOL) plasmas of the reactor vessel.

Experimentally, erosion of PFCs can be elucidated by combining spectroscopic data of material emission during plasma discharges with the results of post-exposure analyses of selected wall tiles removed from the reactor. This way, also the balance between *net* and *gross erosion* can be identified [1]. Here, *gross erosion* refers to the amount of material primarily sputtered from the PFCs while *net erosion* takes into account particles that are re-deposited on the surface. By using marker samples with different geometries and sizes, gross and net erosion can also be extracted from thickness measurements of the markers and analysis of the surrounding areas after a specific plasma experiment as pioneered in the DIII-D tokamak [3,4].

The ASDEX Upgrade (AUG) tokamak is a particularly interesting environment for investigating the erosion characteristics of W [5]. The device operates with full-W PFCs since 2007 [6], in addition to which it has a versatile set of methods for heating the plasmas including neutral beam injection (NBI) and electron cyclotron (ECRH) and ion cyclotron resonance heating (ICRH) sources. In addition, the upgraded divertor manipulator (DIM-II) [7] allows exposing small samples or entire wall tiles in one toroidal sector at the low-field side (outer) strike point region of the AUG divertor. This is the area where the interaction between the plasma and the wall materials are typically the strongest.

Up to now the most important observations related to W migration characteristics are [8–11]: (i) both erosion and migration are strongly dependent on local plasma conditions at the divertor and in the main chamber and especially main-chamber erosion alters the erosion patterns in the divertor, (ii) gross erosion of W is quite well understood and the role of edge localized modes (ELMs) on W sputtering is estimated to be $>$ 50%, and (iii) net erosion is dependent on many parameters including the flux, energy and composition of the background plasma and impinging impurities, local geometry including magnetic and electric fields, surface roughness and morphology of the PFCs, as well as the fuel content and amount of material co-deposited on the surface. In this article, our aim is to provide further insights on point (iii) based on dedicated experiments on AUG and modelling the erosion patterns using the ERO code [12]. The data is obtained from the exposure of special marker samples to a series of well-characterized deuterium (D) plasmas in L-mode.

## 2. Summary of experimental details

### 2.1. Samples and their analyses

The samples exposed on AUG were made of fine-grained graphite and mounted around the pre-determined outer strike-point position on two Mo-coated, bulk-W target tiles of the DIM-II manipulator on AUG. The graphite pieces were coated with a molybdenum (Mo) layer (thickness ~300 nm) on top of which small, rectangular gold (Au) marker spots were produced. The thickness of the spots was ~30 nm and they had two different sizes: $1 \times 1$ and $5 \times 5$ mm$^2$. The smaller ones were designed to assess the gross erosion profile of Au while on the bigger ones also a significant fraction of the eroded particles were assumed to be promptly re-deposited, thus showing net erosion of Au. This was based on our estimate that eroded particles return to the surface after travelling some 1–2 mm in the plasma. In this work, Au was employed as a proxy for W which could not be used as the actual marker material due to the full W coverage of the AUG vessel while Mo gave additional information on the overall shape of the erosion profiles. A photo of the samples before and after their plasma exposure can be seen in Fig. 1a.

Before and after the plasma experiment the samples were analyzed for the thickness of the marker spots and the underlying Mo layer as well as the topography of the sample surfaces. The main analysis tools were Rutherford Backscattering Spectrometry (RBS), Confocal Laser Scanning Microscopy (CLSM), and Scanning Electron Microscopy (SEM) with Energy Dispersive Spectroscopy (EDX). In addition, the composition of the layers formed on the markers and in their immediate vicinity were determined using Nuclear Reaction Analysis (NRA), RBS, and EDX.

### 2.2. Plasma experiments on AUG

The samples were exposed to eight low-confinement mode (L-mode) plasma discharges in D on AUG (AUG shot numbers #35609-35617, #35614 being a failed discharge). The outer strike point was set roughly at the top edge of the lowermost marker samples such that the first few marker spots were located in the private flux region (PFR) and the rest in the SOL, see Fig. 1a. For all the discharges, the flat-top time for the plasma current was $\Delta t \sim 4$ s, the toroidal magnetic field $B_t = 2.5$ T, the plasma current $I_p = 0.8$ MA, the core electron density $n_e \sim 4 \times 10^{19}$ m$^{-3}$, while the auxiliary heating was done by ECRH at the power level of $P_{ECRH} \sim 0.7$ MW. In addition, during the experiment isotopically labelled nitrogen ($^{15}$N) was injected in trace amounts from a valve at the top of the vessel to investigate nitrogen migration at the midplane;

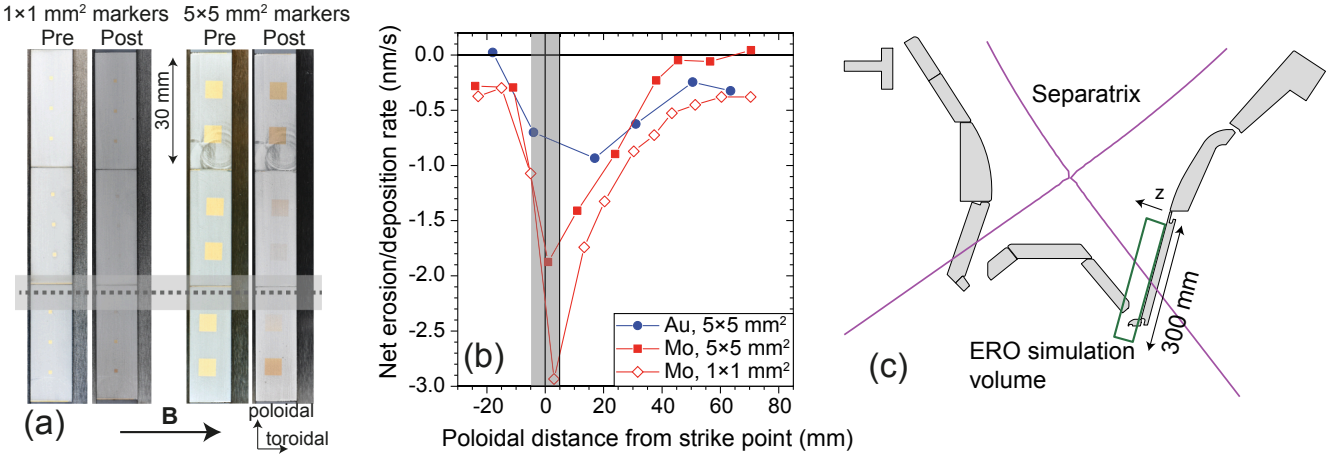


**Fig. 1.** (a) Photographs of marker tiles before (pre) and after (post) their exposure to plasma discharges on ASDEX Upgrade. (b) Experimental net erosion/deposition profiles of Au markers ($5 \times 5$ mm$^2$ spots) and the Mo marker coatings. Here, negative values mean net erosion and positive values net deposition. The gray bar denotes the typical uncertainty of the exact location of the outer strike point. (c) Illustration of the ERO simulation volume (in green) in the ASDEX Upgrade geometry of the discharge #35617. The purple thick line denotes the separatrix, the outer strike point being the point where the separatrix crosses the target surface inside the ERO box. (For interpretation of the references to colour in this figure legend, the reader is referred to the web version of this article.)

residual nitrogen levels were measured also on the marker samples at the divertor region.

Langmuir probe (LP) measurements indicate the electron density to peak to a value of ~5 × $10^{18}$ $m^{-3}$ close to the strike point and exhibit a decay length of 50–60 mm in the SOL. This roughly corresponds to the region where the marker samples were located on the SOL side during the experiment. The electron temperature, for its part, was up to ~20 eV in the vicinity of the strike point and within the first 50–60 mm had only decreased to ~15 eV. The measured LP profiles are shown in Fig. 2a and b for the discharge #35617.

### 2.3. Experimental erosion profiles

The data from the larger Au markers (5 × 5 $mm^2$) indicate noticeable net erosion up to 0.8–1.0 nm/s close to the strike point and ~0.2 nm/s at the top edge of the last marker sample on the SOL side (see Fig. 1b). These erosion rates are 5–10 times higher values than those measured for W after a comparable experiment in [13,14], but the conclusions for the previous experiments were complicated by a large influx of W coming from surrounding PFCs and even the main-chamber regions. By taking into account the discussion in [15] that extra W sources may increase apparent re-deposition by 50%, the true ratio of the net erosion rates of Au and W can be of the order of 3–5. One should note that none of the 5 × 5 $mm^2$ markers were located exactly at the strike point region but poloidally either ~5 mm below or ~20 mm above it, thus the peak value for erosion might be even larger than what Fig. 1b suggests.

Erosion data of the small markers (1 × 1 $mm^2$) does not exist at the time of writing this article. However, some indications of their erosion rates can be extracted from the measured EDX data. For instance, at a distance of 35 mm from the strike point on the SOL side, the relative strength of the Au signal in EDX spectra has diminished by 60–70%, indicating that a substantial fraction of the original marker material has vanished during the experiment.

The eroded and subsequently re-deposited particles seem to be extremely well localized close to their origin. Neither RBS nor SEM/EDX is able to identify any measurable Au inventories outside of the markers. Moreover, no blurring of the edges of the marker spots could be seen in the analysis of SEM results. All this hints that deposition of Au outside their origin is below the detection threshold and that the migration length of the atoms is very short, of the order of 1 mm or less.

Concerning Mo, the erosion peak is qualitatively similar to that of Au but the absolute values, particularly in the strike-point region, can be 2–3 times higher as Fig. 1b shows. Interestingly, larger net erosion for Mo was measured for the samples on which the 1 × 1 $mm^2$ Au marker spots were produced. This could be connected with these samples being mounted on a different target tile, toroidally upstream from the other set of samples (Mo coating and 5 × 5 $mm^2$ Au marker spots), and the two tiles potentially being fixed in a slightly different angle with respect to the magnetic field.

Measurable re-deposition of W (0.05–0.2 nm/s) was observed throughout the samples with peaks on the private-flux region and some 30 mm from the strike-point on the SOL side. Consistently with the observations of higher Mo net erosion on samples with the smaller marker spots, re-deposition of W is also reduced on them by a factor of two: the larger the measured erosion, the higher the plasma flux onto them and the lower the probability for particles to accumulate on them to form deposited layers. The deposition data qualitatively agree with earlier results in [13] and due to the local nature of re-deposition can be attributed to long-range migration of the eroded W.

## 3. Simulation setup for ERO

The erosion results were modelled using the Monte Carlo code ERO (version 1.0) [12]. The code follows particles in a pre-determined simulation volume, covering also the part of the wall where plasma-wall interactions are taking place, until the particles either leave the simulation volume or hit the wall surface without reflecting. In our case, the plasma background (including electron density, electron and ion temperatures, and magnetic and electric fields) is given to ERO in a separate input file.

The simulations were set to cover an area of 300 × 300 $mm^2$ in the poloidal-toroidal plane, corresponding to an entire AUG wall tile in the outer strike-point region and such that the marker samples were located in the middle of the simulation volume, see Fig. 1c and Ref. [15] for details of the applied simulation setup. The box was 50 mm high in the $z$ direction to properly take into account particles returning on the surface after being sputtered or reflected. Non-periodic boundary conditions were used: particles moving outside of the simulation volume were considered lost.

The background plasmas were created using the onion-skin model (OSM) of the DIVIMP code with the SOL option 22 activated and assuming the ion temperature being equal to the electron temperature, i.e., $T_i = T_e$. The different OSM backgrounds were then mapped into the ERO simulation grid. The ERO simulations were performed using three different background plasmas, referred to as "BC", "High-T", and "Low-n", to assess the effect of electron temperature and electron density ($n_e$) on the resulting erosion profiles. The profiles of the three solutions can be found in Fig. 2a and b. One should note that the "Low-n" solution is generated from the self-consistent "BC" profile by applying the same temperature profile and dividing the density profile by a factor of three. In general, the applied profiles give upper and lower boundaries for the true values of $T_e$ and $n_e$, taking also into account that no probe data is available from the exact strike point position; here we extrapolate the peaks to $T_{e,max}$ = 25 eV and $n_{e,max} = 0.8 \times 10^{19}$ $m^{-3}$.

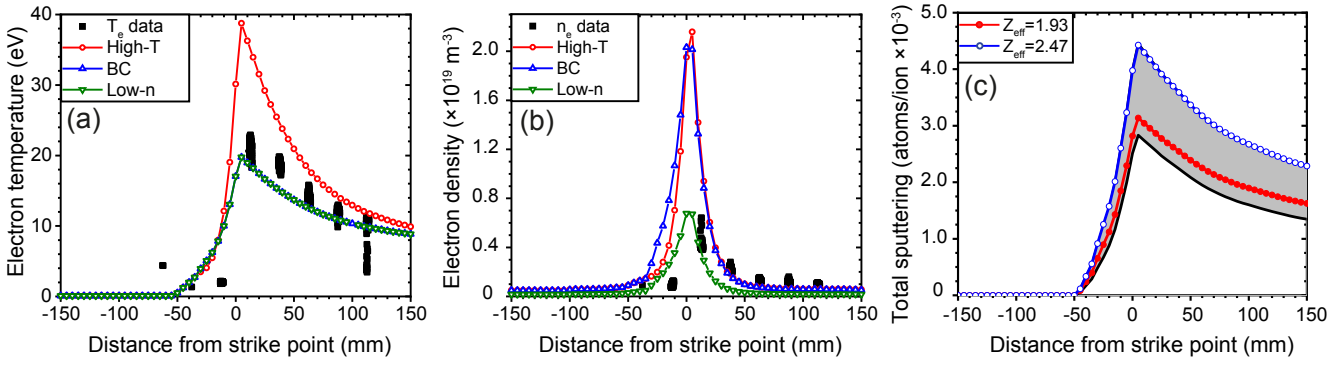


**Fig. 2.** (a,b) Electron (a) density and (b) temperature measured for the AUG discharge #35617 and data from three background plasma solutions used in the ERO simulations as a function of distance from the strike point. (c) Weighted sputtering yield of light impurities (B, C, and N) from Au as a function of distance from the strike point for different combinations of the impurity concentrations with $Z_{eff}$ = 1.93 and $Z_{eff}$ = 2.47 (grey area). The red and blue curves correspond to the cases (i) and (ii) studied in this work. (For interpretation of the references to colour in this figure legend, the reader is referred to the web version of this article.)

The anomalous diffusion coefficient was set to $D_\perp = 1.0\ m^2\ s^{-1}$; the discussion on its effect on the net erosion/deposition profiles can be found in [15]. Finally, the plasma potential and the parallel-B electric field E were approximated by $\Phi = 3k_BT_e/e$ and $\mathbf{E} = -\nabla\Phi$. The sheath model used in our simulations is the standard Brooks model in ERO, consisting of Debye and Chodura components to take into account potential drops in the actual sheath and in the magnetic pre-sheath, respectively [16].

In each simulation, the level of impurities was varied, according to the treatment in [15], such that the concentrations of the light and heavy impurities would correspond to typical values in low-density but high-$T_e$ plasmas of AUG. For the time being, only the effective charge of the different impurities can be experimentally inferred at the outer midplane in the main chamber of AUG. The dominating light elements on the AUG torus are B, C, and N, whose concentrations under conditions relevant for our experiment remain below 1.0 at.%. For W, its concentration is less than 0.01 at.%; see [15] for more details. Because of $^{15}N$ injection (in trace amounts) during the experiment, we assume that the N concentration is the largest of all the three light elements. Boron, for its part, results from regular boronizations of the AUG vessel, however, the experiment was carried out far from a boronization. Also the C concentration is expected to be relatively low since C in the SOL plasma originates from erosion of W-coated graphite PFCs of AUG. The sputtering yield $Y$ induced by nitrogen in its average charge state of $q_{ave} = 5$ is two times stronger than that by boron ($q_{ave} = 3$) and 15–20% larger than the contribution associated with carbon ($q_{ave} = 4$). In our experiment it is thus primarily nitrogen that determines the magnitude of erosion by light impurities unless the concentration of the two other elements is increased to unreasonably high values of several at.%.

In the simulations we considered cases with $c_W = 0.005$–$0.01$ at.% and $c_B$, $c_C$, $c_N = 0.5$–$1.0$ at.%. The most common combinations were (i) $c_W = 0.005$ at.%, $c_B = c_C = 0.5$ at.%, $c_N = 0.75$ at.% and (ii) $c_W = 0.01$ at.%, $c_B = c_C = 0.75$ at.%, $c_N = 1.0$ at.%, corresponding to effective charges of $Z_{eff} = 1.93$ and 2.47, respectively. A set of simulations assuming $c_W = 0$ and the effective charge to $Z_{eff} = 1.66$ were also carried out. The weighted sputtering yield $\sum_i c_i Y_i$of the different light impurities $i$ is shown in Fig. 2c for a range of concentrations corresponding to the effective charges $Z_{eff} = 1.93$ and 2.47; the two named cases (i) and (ii) are denoted by red and blue curves, respectively. At a fixed $Z_{eff}$ the impact of light impurities on sputtering varies in the range of 15–20% as the exact impurity content changes from a strongly boron-dominated situation (lowest yield) to a nitrogen-dominated one (highest yield). Overall, our simulations are able to cover a range where the sputtering yield can be varied by a factor of two.

Each simulation consisted of 50 time steps, corresponding to total simulation time of 10 s, which was enough to reach steady-state erosion/deposition conditions. The simulation grid had a spacing of 1 mm in the toroidal and poloidal directions and set such that at least one grid point would always coincide with the centre of the marker spots. In the $z$ direction, a coarser grid with a spacing of 5 mm was noticed to be sufficient to catch the main physics of the eroded and migrating particles.

## 4. Simulation results

### 4.1. Erosion of Au marker spots

The predicted maximum net erosion of Au is qualitatively consistent with the measurement data. This finding becomes evident in Fig. 3 where the results for both the 5 × 5 mm$^2$ (Fig. 3a) and 1 × 1 mm$^2$ (Fig. 3b) markers are presented for the two pre-determined values of the effective charge ($Z_{eff} = 1.93$ and 2.47) and profiles for the background plasma ("BC" and "High-T"), together with the available experimental data from Fig. 1b. In Fig. 3a, also the effect of density is investigated by reproducing the "Low-n" solution for the case $Z_{eff} = 2.47$).

From the data for the large markers in Fig. 3a, one notices that the strike-point peak of ~0.8–1.2 nm/s ("High-T" background) decreases to 0.1–0.3 nm/s in the private flux region and to <0.05 nm/s in the far SOL. The decrease on the SOL side is slightly faster than what the experimental results in Section 2.3 suggest and quantitatively consistent with the "High-T" solution while in the private-flux region the simulated values overestimate the actual net erosion rates. An additional feature is that the simulated erosion profile shows variations across the marker spots. The validity of the predictions will be checked by microbeam RBS measurements in the near future. Please note that, for technical reasons, the markers in ERO simulations have been set at somewhat different poloidal locations than where they were located in the experiment. This arrangement does not alter the conclusions in this section.

Of the studied parameters, the largest effect on net erosion is attributed to the electron temperature. Around the strike point where the temperature is varied by less than a factor of two ("BC" vs. "High-T"), net erosion values can be up to 2.5–3.0 times larger or smaller. Even small changes can be significant. For example, at around −20 mm, the "BC" and "High-T" profiles in Fig. 2a are inversed compared to other regions and the "High-T" solution also exhibits a steep gradient, and these slight alterations are immediately visible in Fig. 3a. The influence of the electron density, for its part, is weaker as the comparison between the "BC" and "Low-n" curves reveals. Note that all the results are sensitive to the exact location of the strike point: we estimate approximately 10 mm for its uncertainty illustrated by the gray zone in Fig. 1b. Note also that the initial assumption of ion temperature being equal to electron temperature may have resulted erosion being underestimated especially in the "BC" case. However, investigating the effect of varying

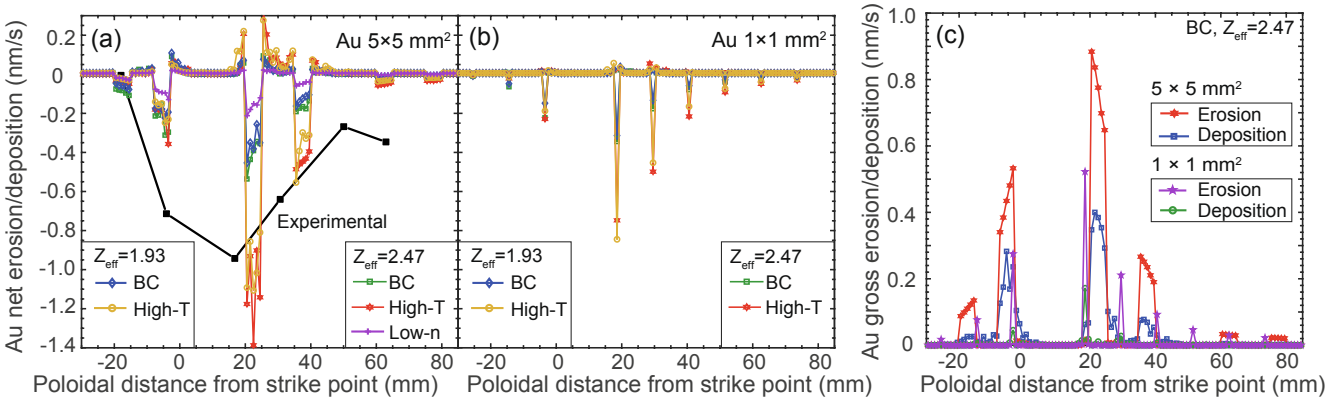


**Fig. 3.** (a,b) Net erosion/deposition profiles for the (a) 5 × 5 mm$^2$ and (b) 1 × 1 mm$^2$ Au marker spots in different simulation cases and (c) gross erosion and deposition of the 5 × 5 mm$^2$ and 1 × 1 mm$^2$ Au marker spots in the "BC" case with $Z_{eff} = 2.47$ as a function of poloidal distance from the strike point. In (a) and (b), negative values mean net erosion and positive values net deposition.

$T_i/T_e$ ratios on erosion and deposition profiles would require recalculating the OSM profiles and is thus left for future studies.

The curves especially in Fig. 3a show sharp net deposition peaks on both sides of each marker spot. The closer they are to the strike point and the higher the electron temperature is, the more prominent they become. According to [15], the net deposition peaks are mainly induced by the **E** × **B** drift, ultimately shifting the gross erosion and deposition profiles with respect to each other. This is evidenced by the gross erosion and deposition profiles shown in Fig. 3c (for the "BC" case). Interestingly, the deposition peaks on the upstream and downstream sides can be equally strong, as has been experimentally observed in [13,14]. Along with drifts, cross-field diffusion (or the absence of it) contributes largely to the occurrence of the measured deposition peaks as investigated in [15].

The effect of impurities on net erosion of Au is within the uncertainties of the input data and assumptions. Only in regions where the electron temperature has dropped below ~ 20 eV (far SOL or private flux region) increasing the impurity content of the plasma leads to enhanced net erosion, typically by < 40%.

The size of the markers appears not to have a large impact on net erosion: according to Fig. 3a and b, the net erosion rates of the 5 × 5 $mm^2$ and 1 × 1 $mm^2$ marker spots match within typical error bars of 10–15%. The clearest exception is the immediate vicinity of the strike point where the erosion rate for the bigger markers is enhanced by 20–25% compared to the smaller spots. The reason for this single point deviating from the overall trend is unknown at the moment but could be connected with the resolution of the applied ERO simulation grid; this will be investigated in detail in the future. On the other hand, gross erosion profiles (Fig. 3c) between the two marker types show distinct differences. In the "BC" case, while for the larger marker spots gross erosion around the strike point is up to 0.7–0.9 nm/s and still 0.2–0.3 nm/s about 20 mm further in the SOL, the corresponding numbers for the small marker spots are 0.5 nm/s and 0.1–0.2 nm/s. This means that re-deposition drops from >50% to <40% when decreasing the marker size from 5 to 1 mm. The lesson learnt is that markers with sub-millimeter dimensions are needed for accurate gross-erosion studies.

### 4.2. Erosion of Mo marker layers

In the case of Mo, the maximum net erosion occurs in the same poloidal region as is the case for Au but this time the simulations strongly underestimate the measured high erosion rates of 2.0–3.0 nm/s (see Fig. 1b): ERO predicts peak values of only 0.1–0.6 nm/s (see Fig. 4a). In addition, hardly any influence of the impurity concentration on net erosion rates is visible. The reason can be connected with the details of the applied background-plasma profiles but also to the specific values selected for the diffusion coefficient and electric field in the ERO simulations. In our earlier work [15], we noticed that either lowering the diffusion coefficient or increasing the electric field, thus enhancing the **E** × **B** drift, the peaks and valleys in the net erosion profile became sharper. Furthermore, the applied non-periodic boundary conditions with particles considering lost after they exit the simulation volume may have had an impact on the results as well as the sheath model used in ERO [16].

Another possibility is connected with the strong re-deposition of the eroded Mo atoms in the simulations. According to Fig. 4b (example shown for the "BC" case), gross erosion is in agreement with the simple mass and charge scaling for the different elements (2–3 times larger for Mo than for Au) but in contrast to Fig. 3c, now >90% of the material appears to be re-deposited. This result can be understood by assuming that everywhere else but on the actual marker spots the substrate material is Mo: it is sufficiently thick that the underlying bulk substrate is not supposed to influence the results. However, it cannot be excluded that the Mo coating on the target tiles is different from that on the marker samples, e.g., because the target tiles have been used in a number of other experiments in the past and been also partially covered with deposited material, including W. Therefore, in practice, the influx of Mo from the surrounding areas would not be that strong as now applied. Future studies include detailed analyses of also the target tiles.

The simulated Mo emission agrees for the most parts with the measured spectral line emissions at 550 nm and gives additional proof that the gross erosion predicted by ERO is of the same order of magnitude as the measurements, particularly when "High-T" simulations are considered. Fig. 4c shows both the measured and simulated line emission (integrated along the *z* axis of the simulation volume) for the AUG discharges #35609, 35610, 35611, and 35613. The gradual decrease of the experimental Mo emission during the plasma experiment can be connected with the erosion of the Mo layer and formation of co-deposits on it. In the far SOL, deviations between experimental and modelling results are the largest, similarly to the discussion of the erosion characteristics. In addition, ERO does not take into account sputtering by fast charge-exchange atoms or any additional features on the surface, both of which may amplify emission compared to the idealistic situation.

### 4.3. Comparing erosion characteristics of Au and W

ERO simulations were also carried out to investigate how differently Au (our proxy) and W (the actual wall material of AUG) would erode in identical plasma conditions on AUG. To this end, the material of the 5 × 5 $mm^2$ and 1 × 1 $mm^2$ markers was changed while otherwise keeping the plasma parameters similar to the ones reported in Sections 4.1 and 4.2. Most of the analyses were executed by setting $Z_{eff} = 1.93$ and using the "High-T" background plasma. Under these circumstances, the caveat is that due to the presence of W impurities, the net erosion rates of the

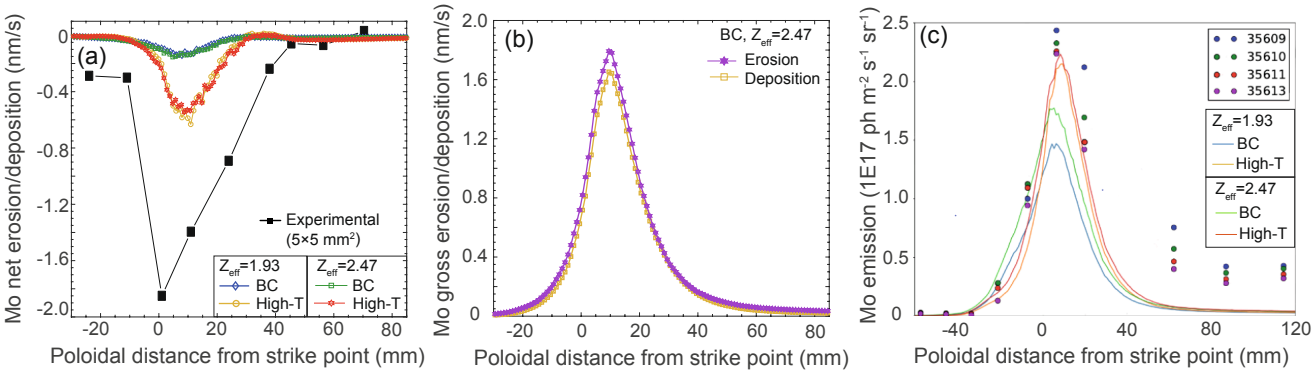


**Fig. 4.** (a) Net erosion/deposition and (b) gross erosion/deposition profiles for the Mo markers in different simulation cases as a function of poloidal distance from the strike point. (c) Experimental and simulated spectral line emissions for Mo at 550 nm as a function of poloidal distance from the strike point in different simulation cases. In (a), negative values mean net erosion and positive values net deposition.

two materials are not fully comparable. In addition, assessing the migration length of the primarily eroded W particles could not be distinguished from the contribution of the background plasma. To overcome these issues, a set of simulations was also carried out without any W in the background plasma, corresponding to $Z_{eff} = 1.66$.

In the case $Z_{eff} = 1.93$, net erosion of Au is estimated to be 3–5 times higher than that of W. This is illustrated in Fig. 5a and b; small differences of the Au profiles from those in Fig. 3 are due to numerical noise. The largest difference is observed in the strike-point region and again the marker size plays a minor role here. Also for W one can see net deposition barriers surrounding markers both on their upstream and downstream sides, in addition to which a noticeable W net deposition region forms between the strike point and the first marker on the SOL side. This is in accordance with the results reported in [15].

In the absence of W impurities, no noticeable changes in the net erosion profiles are observed, only the profiles are altered insignificantly. The clearest impact is the absence of the above-mentioned net deposition region in the interval from 0 to 20 mm.

### 4.4. Migration patterns of the marker materials

The migration of the eroded particles was assessed from 2D profiles where the number of marker particles at the end of each simulation run was reproduced. Examples for Au profiles around the larger marker spots are shown in Fig. 5c and they illustrate that some 70% of the Au particles are deposited within a distance of 10 mm from their origin. Impurities do not alter the situation while a higher electron temperature ("BC" vs. "high-T" case) results in more material being eroded but the deposition profile staying equally local in both cases. For the small marker spots, drawing conclusions is difficult due to a smaller number of particles being available but the shape and the extent of the re-deposited area is very similar to that obtained for the larger markers.

Comparison between W and Au (not shown) does not change the picture: the re-deposition profiles for the two elements are comparable and again a bit more than 70% of both elements can be found within a range of 10 mm from their origin. On the basis of this observation one may infer that the migration lengths of Au and W are similar - only their erosion yields show differences - indicating that the two elements are ionized in a similar fashion. However, one should note that experimentally hardly any Au is observed outside the marker spots but this could mean that the concentrations there are below the sensitivity threshold of SEM/EDX: our simulations show that the absolute number of particles is down by 1–2 orders of magnitude as the distance from the marker spot is more than 1 mm.

## 5. Discussion and conclusions

We have numerically assessed net and gross erosion of Au and Mo on the outer strike-point region of ASDEX Upgrade during a series of L-mode discharges in D with the help of two different types of marker samples, consisting of Au marker spots and Mo marker coatings. Experimental results show net erosion of Au up to 0.8–1.0 nm/s in the strike-point region, which is estimated to be 3–5 times higher than that of W in a comparable experiment by taking into account strong re-deposition of W from other regions. Molybdenum is eroded 2–3 times faster, consistently with predictions by physical sputtering models while the shapes of the erosion profiles of Mo and Au are quite similar. Gross erosion measurements from small markers is still pending and will be discussed in follow-up publications.

The results were simulated using the ERO1.0 code and applying a variety of different background plasmas. The plasmas differed by their electron temperature, electron density, and impurity content. Especially by increasing the electron temperature by a factor of less than two, results in 2.5–3.0 times higher net erosion. This is noticeable since erosion is proportional to the incoming particle flux and the sputtering yield $Y$, i.e., Erosion$\propto n_e T_e^{1/2} Y(T_e)$, where $Y$ is now a strong function of temperature, i.e., $d(\log Y)d(\log T_e) > 1$ in the regime relevant for our experiment. The ion temperature have been assumed to be equal to the electron temperature, while investigating the influence of varying $T_i/T_e$ ratios on the erosion characteristics have been left for future studies. The dependence on density was weaker than that on the temperature while varying the impurity content within the limits characteristic for high-$T_e$ and low-$n_e$ L-mode plasmas on AUG, small effect on the obtained profiles could be seen only in regions where the electron temperature had dropped below 20 eV. Net erosion rates of the two types of marker spots are comparable except for the actual strike-point region, however, re-deposition would drop from >50% to <40% when decreasing the marker size.

The simulated erosion profiles for Mo qualitatively agree with those of Au but underestimate significantly the measured net erosion. This could be due to inaccurate background plasma profiles applied in ERO leading to suppressed gross erosion as well as the electric field being too small and the diffusion coefficient too large. All these would artificially increase re-deposition of the eroded particles but also an optimized sheath model may play a role. In addition, the surrounding areas of the marker samples being covered with impurities and W from previous experiments can lead to re-deposition of Mo becoming significantly smaller than the >90% used in our simulations.

Similarly to the experiments, Au erodes 3–5 times faster than W and the background W here only changes the details of the deposition profiles of W, not the net erosion rate. Some 70% of the particles are

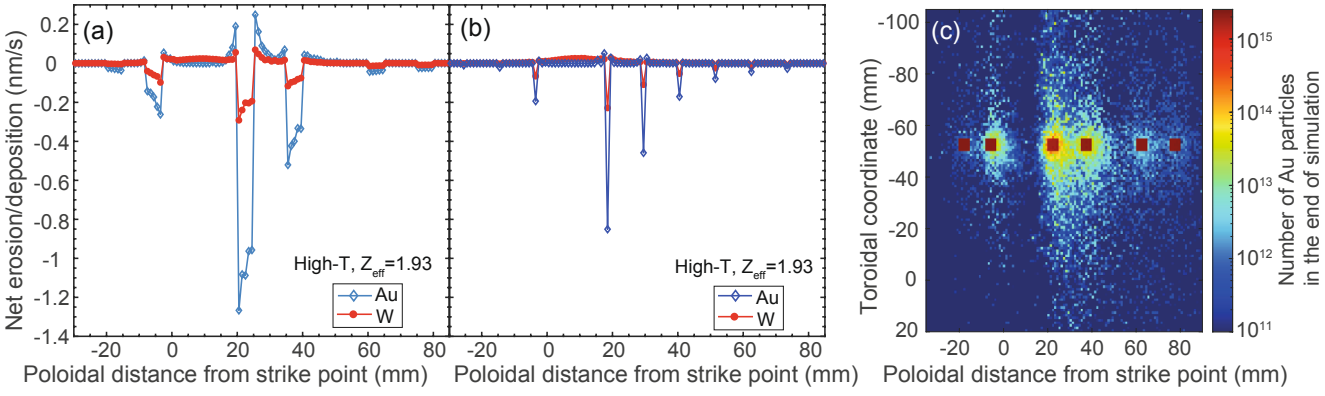


**Fig. 5.** (a, b) Net erosion/deposition profiles for the (a) 5 × 5 mm$^2$ and (b) 1 × 1 mm$^2$ marker spots as a function of poloidal distance from the strike point in the "High-T" case with $Z_{eff} = 1.93$ (with W in the background) by considering the marker spots to consist of Au or W. (c) 2D profile for the number of Au particles in the end of a simulation for 5 × 5 mm$^2$ marker spots in the "High-T" case with $Z_{eff} = 1.66$. In (a) and (b), negative values mean net erosion and positive values net deposition. In (c), the markers are set 50 mm upstream in the toroidal direction to better catch the tail of the particles forming in the downstream direction.

deposited closer than 10 mm from their origin and the migration lengths for the two elements are comparable. This suggests that our analysis is applicable to W as well.

## Declaration of Competing Interest

The authors declare that they have no known competing financial interests or personal relationships that could have appeared to influence the work reported in this paper.

## Acknowledgments

This work has been carried out within the framework of the EUROfusion Consortium and has received funding from the Euratom research and training programme 2014-2018 and 2019-2020 under grant agreement No 633053. The views and opinions expressed herein do not necessarily reflect those of the European Commission. Part of the work performed under EUROfusion WP PFC. The authors would like to thank Dr. Volker Rohde for photographs of the exposed marker samples as well as Prof. Rudolf Neu for preparing the discharge program.

## References

[1] G. Federici, et al., Nucl. Fusion 41 (2001) 1967.
[2] V. Philipps, J. Nucl. Mater. 415 (2011) S2.
[3] P.C. Stangeby, et al., J. Nucl. Mater. 438 (2013) S309.
[4] J. Guterl, et al., Plasma Phys. Control. Fusion 61 (2019), 125015.
[5] H. Meyer, et al., Nucl. Fusion 59 (2019), 112014.
[6] R. Neu, et al., J. Nucl. Mater. 438 (2013) S34.
[7] A. Herrmann, et al., Fusion Eng. Des. 98–99 (2015) 1496.
[8] J.N. Brooks, Fus. Eng. Des. 60 (2002) 515.
[9] R.A. Pitts, et al., Plasma Phys. Control. Fusion 47 (2005) B303.
[10] S. Brezinsek, et al., J. Nucl. Mater. 463 (2015) 11.
[11] R. Dux, et al., J. Nucl. Mater. 390–391 (2009) 858.
[12] A. Kirschner, et al., Nucl. Fusion 40 (2000) 989.
[13] A. Hakola, et al., Phys. Scr. T167 (2016), 014026.
[14] A. Lahtinen, et al., Europhys. Conf. Abstracts 41F (2017) P2.119.
[15] A. Hakola, et al., Nucl. Mater. Energy 12 (2017) 423.
[16] R. Ding, et al., Nucl. Fusion 56 (2016), 016021.